into the origin of the phenomenon of OA. In particular, they allow one to determine the relative roles of the constituent atoms in the structure and thus to suggest how the optical rotation could be modified in a particular crystal.

We thank Professor F. Tuinstra for drawing our attention to the thesis by Reijnhart (1970). We are grateful for a research grant from Jesus College, Oxford, and also to the Science and Engineering Research Council and Plessey Ltd for a JOERS grant, which made this work possible. We also wish to express our gratitude to the referees for their invaluable comments on this work.

References

ABRAHAMS, S. C., GLASS, A. M. & NASSAU, K. (1977). *Solid State Commun.* **29**, 515–516.

ABRAHAMS, S. C., JAMIESON, P. B. & BERNSTEIN, J. L. (1967). *J. Chem. Phys.* **47**, 4034–4041.

ABRAHAMS, S. C., SVENSSON, C. & TANGUAY, A. R. (1979). *Solid State Commun.* **30**, 293–295.

AYRAULT, B., LEFIN, F., LANGLOIS, H., TOUDIC, Y. & PALMIER, J. F. (1972). *Optics Commun.* **5**, 239–243.

BEURSKENS-KERSSEN, G., KROON, J., ENDEMAN, H. J., VAN LAAR, J. & BIJVOET, J. M. (1963). *Crystallography and Crystal Perfection*, edited by G. RAMACHANDRAN, pp. 225–236. London: Academic Press.

BOND, W. L., BOYD, G. D. & CARTER, H. L. (1967). *J. Appl. Phys.* **38**, 4090–4091.

BORN, M. (1922). *Z. Phys.* **8**, 390–417.

BORN, M. & GOEPPERT-MAYER, M. (1933). *Dynamische Gittertheorie der Kristalle.* In *Handbuch der Physik*, Vol. 24, pp. 623–794.

BORN, M. & HUANG, K. (1954). *Dynamical Theory of Crystal Lattices.* Oxford: Clarendon Press.

ENDEMAN, H. J. (1965). *Berekening van de Optische Activiteit van Natriumchloraat en bromaatkristallen en van α-Kwarts.* Dissertation, Utrecht.

EWALD, P. P. (1921). *Ann. Phys. (Leipzig)*, **64**, 253–287.

GLAZER, A. M. & STADNICKA, K. (1986). *J. Appl. Cryst.* **19**, 108–122.

HAMILTON, J. E. (1938). *Z. Kristallogr.* **100**, 104–110.

HERMANN, C. (1923). *Z. Phys.* **16**, 103–134.

KELLERMANN, E. W. (1940). *Philos. Trans. R. Soc. London Ser. A*, **238**, 513–548.

KITTEL, C. (1976). *Introduction to Solid State Physics.* New York: John Wiley.

LAAR, J. VAN, ENDEMAN, H. J. & BIJVOET, J. M. (1968). *Acta Cryst.* A**24**, 52–56.

LANDOLT-BÖRNSTEIN (1962). *Zahlenwerte und Funktionen*, Band II. Berlin: Springer.

LANDOLT-BÖRNSTEIN (1979). *New Series*, Vol. 11. Berlin: Springer.

LENZO, P. V., SPENCER, E. G. & BALLMANN, A. A. (1966). *Appl. Opt.* **5**, 1688–1689.

LOWRY, T. M. (1935). *Optical Rotatory Power.* London: Longmans.

NATH, G. & HAUSSÜHL, S. (1969). *Appl. Phys. Lett.* **14**, 154–156.

REIJNHART, R. (1970). *Classical Calculations Concerning the Double Refraction, Optical Rotation and Absolute Configuration of* Te, Se, *Cinnabar* (HgS), *α- and β-Quartz, β-Cristobalite,* $NaNO_2$, $NaClO_3$ *and* $NaBrO_3$. Dissertation, Delft.

SCHWARZENBACH, D. (1966). *Z. Kristallogr.* **123**, 161–185.

STADNICKA, K., GLAZER, A. M. & MOXON, J. R. (1985). *J. Appl. Cryst.* **18**, 237–240.

SVENSSON, C., ABRAHAMS, S. C. & BERNSTEIN, J. L. (1979). *Acta Cryst.* B**35**, 2687–2690.

SZIVESSY, G. & MÜNSTER, C. (1934). *Ann. Phys. (Leipzig)*, **20**, 703–726.

TESSMAN, J., KAHN, A. & SHOCKLEY, W. (1953). *Phys. Rev.* **92**, 890–895.

Acta Cryst. (1986). A**42**, 569–577

Convergent-Beam Reflection High-Energy Electron Diffraction (RHEED) Observations from an Si(111) Surface

BY G. LEHMPFUHL

Fritz-Haber-Institut der Max-Planck-Gesellschaft, Faradayweg 4-6, *D*-1000 *Berlin* 33, *Federal Republic of Germany*

AND W. C. T. DOWELL

CSIRO Division of Chemical Physics, Clayton, Victoria, Australia

(*Received* 26 *March* 1986; *accepted* 18 *July* 1986)

Abstract

Conditions for the intensity enhancement of a Bragg reflection are investigated through convergent-beam (CB) reflection electron diffraction experiments. This intensity enhancement is of great interest for reflection electron microscopy of surfaces. Comparison of CB reflection diffraction patterns with CB transmission diffraction patterns shows a very similar enhancement which can be explained by Bloch waves. The observed surface diffraction parabolae are closely related to Kikuchi envelopes. The intensity enhancement can be interpreted as a channelling phenomenon.

0108-7673/86/060569-09$01.50

Introduction

Over the last few years, the reflection electron microscopy (REM) method has been used successfully for studying the topography of single-crystal surfaces. This application was introduced by Højlund-Nielsen & Cowley (1976). The investigations require, in addition to well defined smooth crystallographic surfaces, very clean vacuum conditions, otherwise observation will be disturbed by contamination. In order to fulfil these requirements, the experiments must be performed in ultra-high vacuum (UHV), as shown by Osakabe, Tanishiro, Yagi & Honjo (1980), or at least under UHV-similar conditions in the specimen chamber (Hsu & Cowley, 1983).

The resolution in REM is limited by foreshortening owing to the grazing incidence of the electrons. Increasing the angle of incidence reduces the foreshortening but decreases the image intensity. From reflection high-energy electron diffraction (RHEED) it is known that Bragg reflection can show an intensity enhancement for distinct directions of the incident beam (Kohra, Molière, Nakano & Ariyama, 1962). In recent investigations of surface treatments by REM such an enhanced Bragg reflection was used for imaging, leading to an increase of intensity and to higher contrast of the surface structure (Uchida, Lehmpfuhl & Jäger, 1984).

The intensity enhancement of a Bragg reflection can be investigated using the convergent-beam RHEED technique (CB-RHEED), as shown in an earlier paper (Ichimiya, Kambe & Lehmpfuhl, 1980). With this technique a large area of reciprocal space is displayed all at once in different diffraction spots, which allows easier comparison with theoretical considerations. In particular, many-beam interactions can clearly be seen. However, contamination in the ordinary high vacuum has, up to now, prevented more detailed investigation. Already a few monolayers of hydrocarbon molecules would prevent observation of a RHEED pattern from a smooth surface. We have found that the specimen contamination caused by the interaction of the small electron probe with the carbon hydrogen molecules on the surface can be cut down to a negligibly low value if the specimen area, and the specimen itself, is cooled to below 173 K in a normal vacuum instrument (Dowell & Williams, 1980). These conditions permit undisturbed CB-RHEED investigations. Recently Shannon, Eades, Meichle & Turner (1985) reported CB-RHEED zone-axis patterns from surfaces of MgO and MoS_2 using a Philips EM 420 transmission electron microscope. During the analysis of our experimental results we found that the intensity enhancement which was related to surface-state resonance is not confined to the surface. In the present investigation we examine CB-RHEED and show to what degree analogy can be made with transmission electron diffraction (TED) with regard to electron channelling.

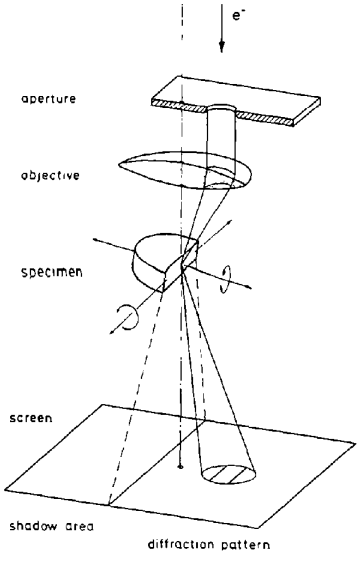

Fig. 1. Schematic ray diagram for convergent-beam reflection electron diffraction.

Experiment

We have performed CB-RHEED experiments with a convergent-beam diffraction camera which allows specimen cooling down to 100 K, as described by Dowell & Williams (1980). A small Si crystal with a (111) cleavage face was mounted on the goniometer stage and inserted in the back focal plane of the objective lens as shown in Fig. 1. The (111) cleavage face with dimensions of about $1{\cdot}0\times0{\cdot}3$ mm was obtained by cleavage from a (111) Si wafer. The angle between the two (111) faces is $\sim 70{\cdot}53°$. This crystal was glued with conducting silver onto the specimen stage. The specimen could be rotated approximately $\pm 15°$ about two axes. The cleavage face was nearly parallel to the optical axis of the lens. Direction and cone angle of the incident electron beam were determined by the position and size of the aperture in front of the objective lens. In this arrangement the specimen is placed outside the field maximum of the objective lens, which is not possible using a condenser objective lens (Uchida, Jäger & Lehmpfuhl, 1984). In the latter case one expects perturbations in the diffraction pattern in CB-RHEED owing to image rotation which depends on the z position (along the optical axis) of the specimen part contributing to the diffraction pattern.

Results

Reflection diffraction

A large-angle convergent-beam RHEED pattern from the Si(111) surface close to the [112] azimuth is shown in Fig. 2. We call such a pattern (after

Goodman, 1972) a Kossel pattern for electrons. It resembles a Kikuchi pattern; however, it is produced mainly by elastic scattering of the primary electrons. Owing to inelastic processes, a faint Kikuchi pattern is superimposed showing a similar intensity distribution. The bright lines parallel to the shadow edge are the different diffraction orders of Bragg reflection from the (111) surface. Because of refraction the 111 and 222 lines are not visible, and the 333 reflection line is close to the shadow edge. The straight lines correspond to Kikuchi lines from lattice planes (sometimes they will also be called 'Kikuchi lines') while the curved lines describe parabolae which can be understood as surface diffraction effects. They bear some similarities to the Kikuchi envelopes which are observed in transmission diffraction, as will be discussed later.

The surface diffraction parabolae have already been described in an earlier paper (Ichimiya, Kambe & Lehmpfuhl, 1980). However, we shall, for reasons of convenience, repeat the derivation in order to compare them with experimental observation. Thus we show in Fig. 3 a schematic ray diagram in reciprocal space for the RHEED situation from a flat crystal surface where the reciprocal-lattice points lie on rods perpendicular to the surface [Fig. 2 of Ichimiya, Kambe & Lehmpfuhl (1980)]. The intersection circle of the Ewald sphere with the plane containing the rods is indicated. $\mathbf{B}_m$ is a vector within this plane perpendicular to the rods and pointing from the origin to the rod m. In our considerations we neglect the influence of the mean inner potential. We consider diffraction conditions for such directions of the incident beam where the intersection circle of the Ewald sphere in Fig. 3 just touches a rod. The centre of this circle is the projected centre of the Ewald sphere. Under this condition a wave with wave vector $\mathbf{K}_m$ is excited which travels in a direction parallel to the crystal surface. This may lead to an enhanced intensity of the specular reflected beam. All possible directions of incidence which fulfil this condition can be found by the construction shown in Fig. 4 [corresponding to Fig. 3 of Ichimiya, Kambe & Lehmpfuhl, (1980)]. Here, the intersection circles of the Ewald sphere with the plane containing the rods in Fig. 3 are shown for five different directions of incidence just touching the rod $m \triangleq \bar{2}20$. The projection of the centres of the Ewald sphere lie on a parabola with the coordinates X and K_{on}, which may be obtained from a simple geometric consideration:

$$K_{on}^2 + X^2 = (X + B_m)^2, \qquad (1)$$

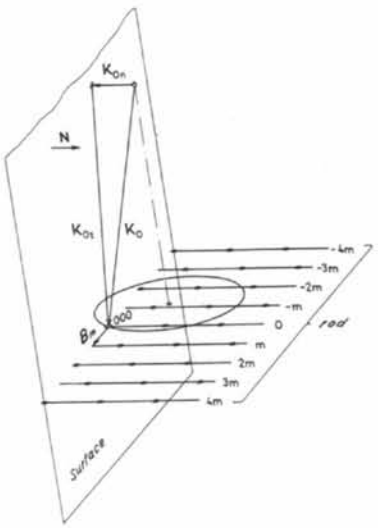

Fig. 3. Schematic diagram for a RHEED situation from a flat single-crystal surface. The reciprocal-lattice points are replaced by reciprocal rods perpendicular to the surface. $\mathbf{K}_0$ is the wave vector of the incident beam. The intersection circle of the Ewald sphere with the plane containing the rods is indicated. $\mathbf{B}_m$ is a vector in reciprocal space pointing from the origin perpendicular to a rod m (Fig. 2 of Ichimiya, Kambe & Lehmpfuhl, 1980).

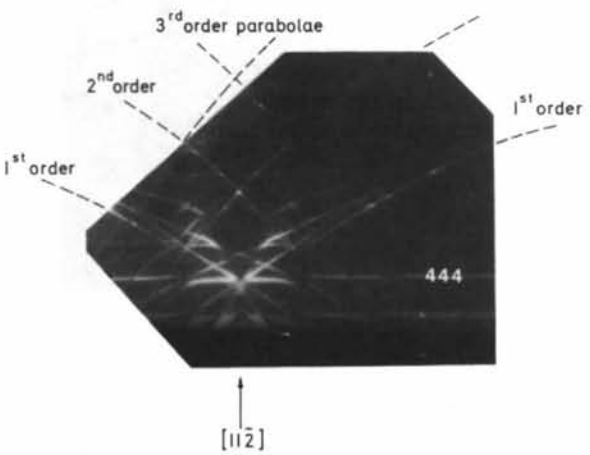

Fig. 2. Wide-angle CB-RHEED pattern (Kossel pattern) from an Si(111) surface at [11$\bar{2}$] azimuth. For indexing of Kikuchi lines and parabolae see Fig. 5.

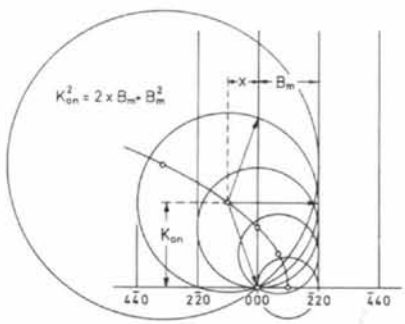

Fig. 4. Intersection circles of the Ewald sphere with the reciprocal plane containing the rods and the origin for such directions of incidence where the Ewald sphere touches the first rod. The projected centres of the Ewald sphere are lying on a parabola which obeys equation (2) (Fig. 3 of Ichimiya, Kambe & Lehmpfuhl, 1980).

leading to

$$K_{on}^2 = 2B_m X + B_m^2, \tag{2}$$

the equation for a parabola with

$$X = -\tfrac{1}{2}B_m \quad \text{for} \quad K_{on} = 0 \tag{3}$$

and

$$|K_{on}| = |B_m| \quad \text{for} \quad X = 0. \tag{4}$$

The question now is how to identify the parabolae in the Kossel pattern. The parabolae describe the position of the projection of the centres of the Ewald sphere in the diffraction plane. Kikuchi or Kossel patterns are fixed with the orientation of the crystal. They are produced by scattering from the crystal net planes. The pairs of Kikuchi lines are parallel to these planes. The extended planes would intersect the diffraction pattern half-way between the line pairs as given by the broken lines in Fig. 5. The horizontal and vertical broken lines are the traces of the extended (111) and $(\bar{1}10)$ net planes. They intersect along the $[11\bar{2}]$ zone axis (which starts in the crystal). If the crystal is rotated the Kikuchi pattern (corresponding to the schematic diagram in Fig. 5) moves on the screen in the same sense.

In addition to the Kikuchi pattern, one has to consider the reciprocal space with an origin which is defined by the wave vector of the incident beam (which is not visible in the diffraction pattern). This wave vector itself is defined in the Kikuchi pattern by its projection with an origin in the intersection point of the two broken straight lines in Fig. 5 [the traces of the (111) and $(\bar{1}10)$ planes]. The wave vector of the incident beam is mirror reflected by the (111) plane. Thus the parabola of (2) can be constructed in the schematic diagram of Fig. 5 with X and K_{on} as coordinates along the traces of the (111) and $(\bar{1}10)$ planes, respectively. The zero point is the intersection of the two traces, the position of the $[11\bar{2}]$ zone axis.

The parabolae are calculated for the $[11\bar{2}]$ azimuth with $|B_m| = |\bar{2}20|$ (first order) and $|\bar{4}40|$ (second order) and shown schematically in Fig. 5, together with some Kikuchi lines (or Kossel lines). The schematic diagram was fitted to experimental observation for the higher-order Kikuchi lines 777 and 888, which are negligibly displaced by refraction. The calculated parabolae are then in excellent agreement with the experimental observation in Fig. 2. For small values of $|K_{on}|$ they show a little deviation due to the refraction effect. A double contour of the parabolae is partially produced by segments of Kikuchi lines.

For low glancing angles of scattered waves a strong dynamical interaction can be seen in Fig. 2 from the missing intensity for special directions of incidence. Especially near the $[11\bar{2}]$ azimuth close to the shadow edge a strong dynamical interaction of simultaneous scattering from the (111) plane together with the $(\bar{1}31)$ and $(3\bar{1}1)$ planes can be seen. The intensity distribution along the 555 Kikuchi line or along the 666 and 777 Kikuchi lines near the $[11\bar{2}]$ azimuth is also strongly influenced by dynamical effects in the area where the two parabolae of second order intersect.

The influence of the surface can best be seen when using a convergent beam with a small cone angle as for a Kossel–Möllenstedt-type pattern. This is achieved by a small aperture in front of the objective lens. Under this condition a smaller area of the specimen, of the order of 100 by 5000 Å, is irradiated by

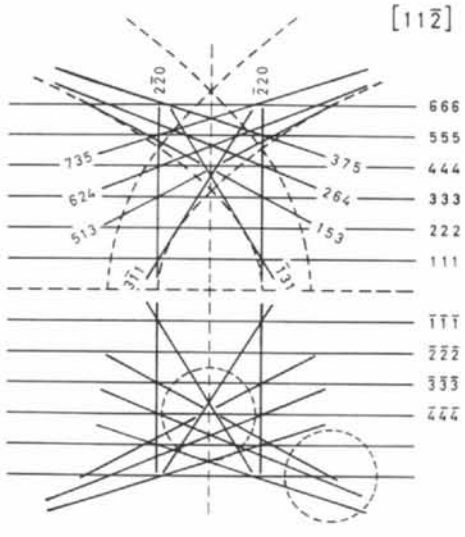

Fig. 5. Schematic diagram of some Kikuchi lines and surface diffraction parabolae of first and second order for diffraction from the (111) surface near the $[11\bar{2}]$ zone axis. The cones of the incident convergent beam for two different directions of incidence are indicated by the dotted circles corresponding to the diffraction conditions shown in Fig. 6 (left circle) and Fig. 7 (right circle).

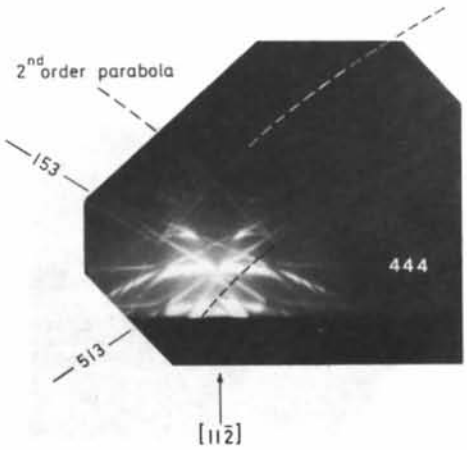

Fig. 6. CB-RHEED pattern of Kossel–Möllenstedt type from the Si(111) surface near the $[11\bar{2}]$ azimuth. The cone of the incident beam is limited by an aperture. The position of the illuminating cone is indicated by one of the dotted circles in Fig. 5. The dotted curve indicates one of the surface diffraction parabolae described by equation (2).

the convergent beam with a cone angle of just $1{\cdot}5\ \theta_{111}$. (The probability of finding a smooth area with only a few steps increases with decreasing size of the area. Distortion of the reflection diffraction pattern by transmission diffraction is reduced. Without an aperture the irradiated area is much larger, of the order of micrometers, owing to spherical aberration.) Fig. 6 shows such a CB-RHEED pattern. The excitation condition is shown in Fig. 5 by the left dotted circle. The cone of the incident beam covers directions of incidence for the excitation of the 333, 444 and 555 lines. This is an unusual diffraction pattern, deviating from the normal convergent-beam pattern in transmission because of mirror reflection. Electrons within the cone of incidence along the $\bar{3}\bar{3}\bar{3}$ lines are reflected to the 333 line, and along the $\bar{4}\bar{4}\bar{4}$ line to the 444 line, *etc.* The shape of the cone of incidence is mirror reflected in the diffraction pattern.

The lines outside the reflected cone of incidence are mainly Kikuchi lines from inelastic scattering of the electrons. The unexpected strong intensity along the 513 and 153 lines within the small cone of reflection is caused by surface diffraction, and also the strong intensity between the parabolae and the $3\bar{1}1$ and $\bar{1}31$ Kikuchi lines near the 333 line. Marten & Meyer-Ehmsen (1985) reported on the investigation of resonance effects from Pt(111) using the rocking-beam technique. For their investigations such a CB-RHEED pattern would have been very helpful in testing the theoretical model calculations of reflected intensities.

Enhancement of the intensity of a Bragg reflection can already be seen in the Kossel pattern in Fig. 2 along the first-order parabola due to $|B_m| = |\bar{2}20|$ when crossing the Kikuchi lines 666 or 777. This effect can be seen much more clearly in the CB-RHEED pattern shown in Fig. 7, taken with a small aperture in a position indicated in Fig. 5 by the right dotted circle. The surface diffraction parabola crosses the 666 Kikuchi line. The intensity is enhanced at the crossing point. Along the parabola the intensity is similar to the intensity along the 666 Kikuchi line. For the diamond structure the 666 reflection is forbidden; however, owing to dynamical interaction, a noticeable intensity can be observed, as for 555 *etc.* The intensity enhancement is of the order of a factor of five compared with the Bragg intensity, and compared with a mirror reflection from the (111) surface the enhancement is even higher.

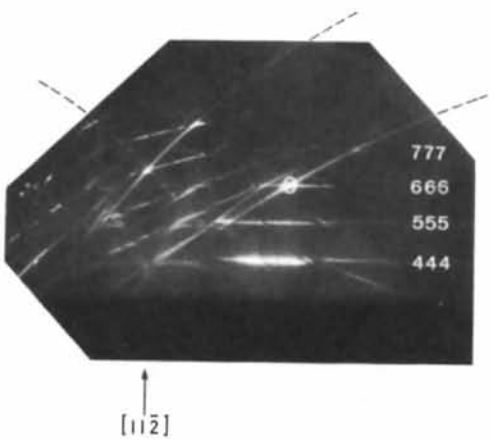

Fig. 7. CB-RHEED pattern of Kossel–Möllenstedt type from Si(111) near the [11$\bar{2}$] azimuth showing intensity enhancement of the 666 reflection at the intersection of the 666 Kikuchi lines with the surface diffraction parabola. The position of the cone of incidence is indicated by a dotted circle in Fig. 5. The enhancement area is circled in white.

Similar intensity enhancements are observed at crossing points of the parabola with the higher-order Kikuchi lines as 777, 888 *etc.* (not shown). These are of great interest for surface imaging in reflection electron microscopy (REM). Using such an enhanced reflection for REM, deviations from an undistorted flat surface can be imaged with high contrast. Close to the [11$\bar{2}$] zone axis the intensity distribution shows a very complicated characteristic structure, and the enhancement is not so pronounced.

Transmission diffraction

For high diffraction angles the surface diffraction parabolae are closely related to the Kikuchi envelopes which are observed in transmission electron diffractions. In Fig. 8 is shown the convergent-beam transmission diffraction pattern of the diffraction condition of Fig. 7. The size and position of the cone of the incident convergent electron beam are indicated by the dotted circle. We recognize the Kikuchi envelopes which correspond to the parabolae of first and second order in Fig. 5. The envelopes can clearly be seen as the tangents of sequences of Kikuchi lines as well as curved lines. They are slightly different from the surface diffraction parabolae. Their intensity is less than the intensity along the 666 line. However, the intensity enhancement is also observed at the intersection points with the higher-order reflections from the (111) plane, as 666 in Fig. 8. The intensity distribution around this intersection is very similar to the RHEED observation. In this case again a diffracted beam is excited which lies in the (111) plane. This means that the electron current density distribution is concentrated in the (111) planes along the atom rows in the [11$\bar{2}$] direction (also leading to an enhanced background). Marten & Meyer-Ehmsen (1985) called this effect 'monolayer resonances' for a surface. Von Laue (1948) had already pointed to the close relation between Kikuchi envelopes and diffraction from a surface.

Because of the similarity between the two diffraction situations in transmission and in reflection we can try to estimate the current density distribution in the surface region of the crystal in the case of

reflection by a calculation of the current-density distribution in the (111) plane of the bulk crystal. Furthermore, we can calculate the diffraction intensity along the 666 Kikuchi line near its intersection with the envelope and compare it with the intensity distributions in the CB transmission and reflection patterns.

This was done in a many-beam calculation using the Bethe formalism in the form described earlier (Lehmpfuhl & Reissland, 1968). The characteristic intensity dependence on azimuth was already visible in a ten-beam approximation. However, details were better reproduced with a higher approximation. It was found that consideration of thirty beams was sufficient. The calculations were performed for two different thicknesses of 1000 and 2000 Å taking absorption into account. Parameters for the imaginary potential were taken from experimental data (Voss, Lehmpfuhl & Smith, 1980). In Fig. 9 the azimuthal dependence of the calculated 666 intensity is shown together with a densitometer trace along the 666 Kikuchi line in Fig. 8. The intensity modulation agrees with the experimental observation in transmission and approximately with the intensity distribution in reflection in Fig. 7. The characteristic intensity enhancement can clearly be seen (for both thicknesses) at an azimuth given by $H = -5{\cdot}0$. This azimuth expresses the angle of the incident beam against the $(\bar{1}10)$ plane expressed in units of a Bragg angle $\theta_{\bar{1}10}$ which means, for example, that for $H = -4{\cdot}0$ the $(4\bar{4}0)$ interference is exactly excited.

In order to get a deeper insight into the physical reasons for the intensity enhancement in transmission, we consider the partial waves of the strong Bloch waves and their eigenvalues. The difference in the eigenvalues of the two main Bloch waves of a high-order reflection is very small, especially for the forbidden 666 reflection of silicon. The amplitudes of two 666 partial waves have opposite sign. Owing to the small differences of their eigenvalues, the extinction length of 100 keV electrons is approximately 18 500 Å. The intensity increases only very slowly with thickness but will be reduced simultaneously by absorption. Thus the intensity of 666 will be very low except for orientations where other reflections are excited - especially a reflection with a wave vector lying in the (111) plane. This is simply the condition for deriving the parabola equation (2), which can also be understood as *Umweganregung*. In the experiment we see this as the intersection of the envelope with the 666 Kikuchi line. In this case a third Bloch wave is strongly excited. In Fig. 10 the azimuthal dependence of the eigenvalues of significant Bloch waves is shown near the azimuth for intensity enhancement. This is a section through a few branches of the dispersion surface. They belong to the 666 excitation (the horizontal eigenvalue pairs) and to the 153 excitation (oblique lines). At the intersection of the different branches three strong Bloch waves are excited with distinctly different eigenvalues. Strong enhancement is observed at $H = -5{\cdot}0$. The corresponding amplitudes of the 666 partial waves with their signs and eigenvalues are indicated in the

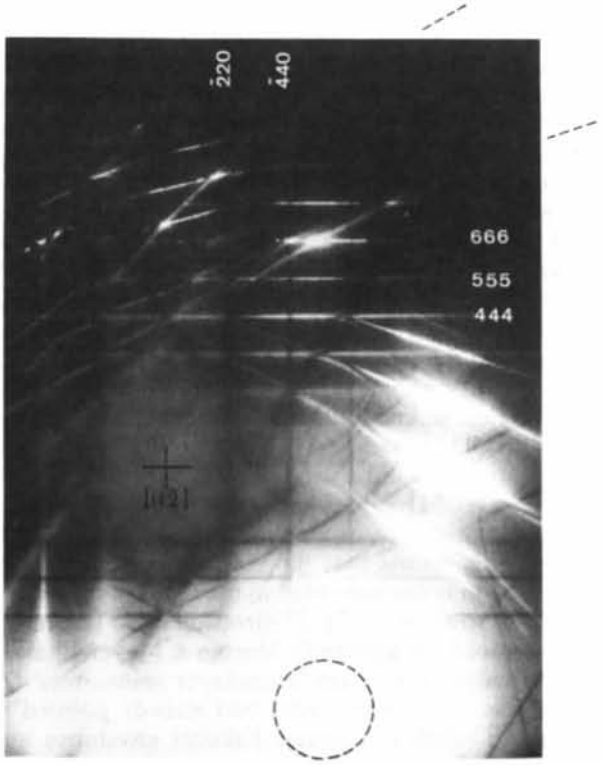

Fig. 8. Kossel-Möllenstedt pattern in transmission from Si(110) plate seen near the $[11\bar{2}]$ azimuth showing a similar enhancement of the 666 reflection to Fig. 7. The Kikuchi envelopes correspond to the surface diffraction parabolae. The position of the cone of incidence is indicated by the dotted circle.

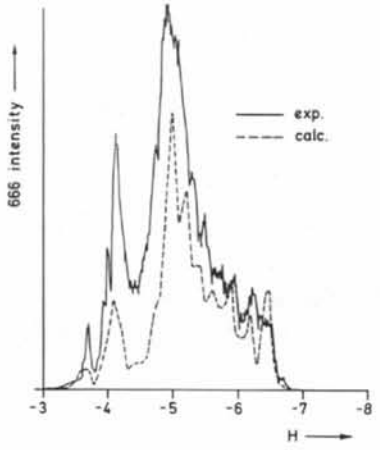

Fig. 9. Intensity distribution along the 666 Kikuchi line in Fig. 8, broken line calculated for 2000 Å thickness, full line densitometer trace. Maximum of enhancement at $H = -5{\cdot}0$. H characterizes the azimuth of the 666 interference expressed by an angle of the incident beam against the $(\bar{1}10)$ plane in units of a (110) Bragg angle.

inset to Fig. 10. The larger difference in eigenvalues results in a reduced extinction length. After a thickness of about 1850 Å an intensity maximum of the 666 reflection is observed. This would explain the observation of double contours of atomic steps on the Si (111) surface in a reflection electron microscope image under such a condition for the direction of the incident electron beam (Lehmpfuhl & Uchida, 1986). Fig. 10 shows also that one should expect an intensity enhancement at $H = -4{\cdot}0$, in agreement with the intensity profile in Fig. 9. This explains the occurrence of the double parabolae.

Similar behaviour is found for the enhancement of the 777 and 888 reflections, *etc.* The 555 reflection does not show an enhancement because the corresponding reflection 042 in the (111) plane is forbidden.

The intersection point of the Kikuchi envelope with the 666 Kikuchi line in Fig. 8 lies exactly halfway between the two vertical Kikuchi lines $\bar{4}40$ and $\bar{6}60$ corresponding to $H = -5{\cdot}0$. From geometric considerations one would expect the enhancement at $H = -4{\cdot}75$ which corresponds to the exact excitation of the 153 reflection together with 666. This shift can immediately be understood by the intersection of the dispersion surfaces, as shown in Fig. 10. A similar shift is also observed in the case of the intensity enhancement of 777, 888 *etc.*

The physical reason for the intensity enhancement can be seen by considering the electron density distribution in the strong Bloch waves. In Fig. 11 the density of each of the three strong Bloch waves is projected onto the $(11\bar{2})$ plane for the enhancement situation ($H = -5{\cdot}0$). Two Bloch waves are strongly modulated in and perpendicular to the (111) plane. One of them shows density maxima also at the atom positions, while the other shows density maxima only between the atom rows. A third Bloch wave is modulated only perpendicular to the (111) planes with density minima in the atom planes. The absorption coefficients of the three Bloch waves vary only slightly. The Bloch wave with density maxima at the atom rows has the larger absorption coefficient, $4{\cdot}4 \times 10^{-3}$ Å^{-1}, while the two others have the smaller value of $4{\cdot}1 \times 10^{-3}$ Å^{-1}. The resulting current-density distribution at the exit surface of the crystal is obtained by coherent superposition of the electron density distribution of the different Bloch waves.

Considering the different density distributions, one finds projected areas which contain densities of only one Bloch wave. This results in thickness-independent current-density maxima within the projected area. The thickness-independent concentration of the current-density distribution along and parallel to the atom rows can be understood as channelling. At another azimuth such as $H = -4{\cdot}5$ two Bloch waves exist with slightly different eigenvalues, which are only weakly modulated perpendicular to the (111) planes. They give rise to a weak reflection.

Surface diffraction parabolae can be observed also for other azimuths such as $[21\bar{3}]$, $[31\bar{4}]$, $[41\bar{5}]$ *etc.* However, they are not important for REM because of the small enhancement of the Bragg intensities. They can be seen in transmission as well. As an example, reflection and transmission patterns in a convergent beam are shown in Fig. 12 for the $[21\bar{3}]$ azimuth showing again a striking similarity. The ordinate of the intersection point of the parabola pair allows identification of the azimuth according to (4).

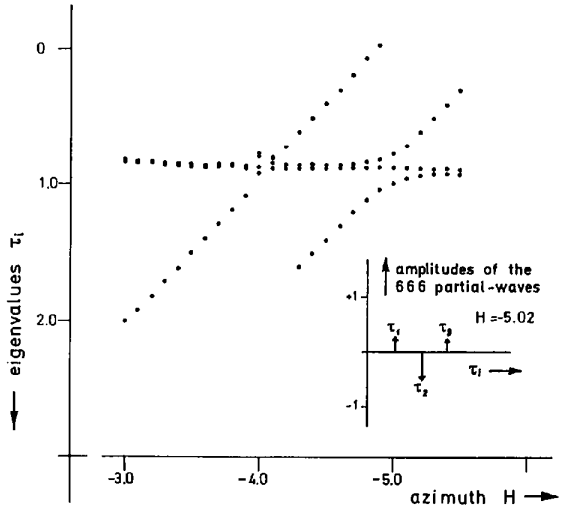

Fig. 10. Azimuthal dependence of four branches of the dispersion surface for 666 excitation near the intensity enhancement. The inset shows the eigenvalues and the 666 amplitudes of the three significant Bloch waves at $H = -5{\cdot}0$.

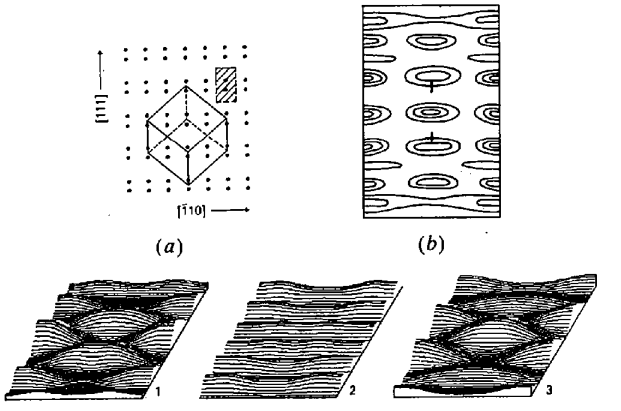

Fig. 11. Electron density distribution in the three significant Bloch waves of Si at $H = -5{\cdot}0$ in Fig. 10 around the double row of atoms in $[11\bar{2}]$ projection as shown in (*a*). The density was calculated for the hatched area. The positions of the atom rows are indicated by crosses in (*b*). Here the thickness-independent current-density distribution of the three Bloch waves is shown. In the [111] direction the scale is enlarged in order to give a better display of the density distribution.

All these facts described by the Bloch wave picture are clearly seen in the CB-TED patterns. They are also found in the CB-RHEED patterns for scattering angles above the 555 excitation. Deviations, however, are observed for small scattering angles such as 333 or 444 which can only be interpreted by a complicated surface diffraction calculation shown earlier (Ichimiya, Kambe & Lehmpfuhl, 1980). In spite of the fact that in the case of RHEED the Bloch wave treatment is modified with respect to TED by the different boundary conditions, the similarity of the intensity distributions in both cases (compare Figs. 7 and 8) does encourage us to tentative interpretation of the intensity enhancement in RHEED as caused by the same mechanism as in the case of TED, namely electron channelling. It is indeed surprising to find a good qualitative description of the RHEED intensity distribution by a Bloch wave treatment in transmission. The above mentioned double contours of monoatomic steps on Si in REM could also be explained by this treatment. Of course, for a quantitative analysis of the RHEED intensity distributions, dynamical surface diffraction calculations have to be performed properly. This will prove whether our interpretation of the scattering process is correct or not, and will correctly reproduce the scattering behaviour at small angles.

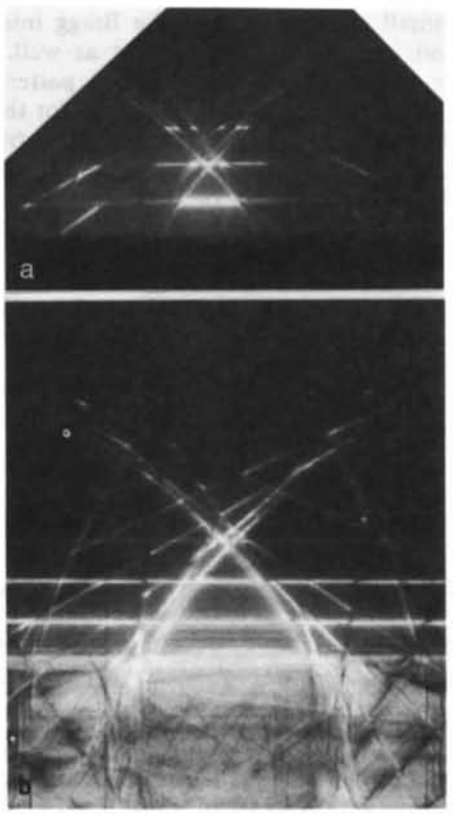

Fig. 12. Comparison of surface diffraction parabolae with Kikuchi envelopes of Si near the [21$\bar{3}$] azimuth; (*a*) CB reflection electron diffraction, (*b*) CB transmission electron diffraction.

Concluding remarks

Intensity enhancement of a high-order reflection from a low-indexed lattice plane is observed in the case of a simultaneous excitation of a wave within this plane. This enhancement is not bound to the surface. Only at grazing incidence can a surface-specific enhancement of a Bragg reflection be observed which is understood as surface resonance. However, such a reflection will not be useful in reflection electron microscopy because of the strong foreshortening effect with its concomitant reduction in resolution. The similarity between the surface diffraction parabolae and the Kikuchi envelopes allows an estimation of the current-density distribution in the surface by bulk calculations of Bloch waves, and allows a better understanding of the physical background of this effect. From these considerations the Bragg intensity enhancement can be understood as a channelling phenomenon which can also be expressed as *Umweganregung*. Furthermore, the occurrence of the double parabolae in surface diffraction can be explained by the 'intersection' of significant branches of the dispersion surface. Since channelling in the bulk and in the surface depends on the direction of the incident electron beam, there may exist a possibility of localization of an adsorbate by combining electron loss spectroscopy with convergent-beam RHEED (Taftø & Lehmpfuhl, 1982).

We express our gratitude to Dr K. Kambe for many fruitful discussions and suggestions and we thank Dr P. Goodman and Dr A. Smith for a critical review of the manuscript. We thank D. Williams for refining the convergent-beam diffraction camera and for assistance during the experiments, and D. Müller for assistance during the analysis of the data. We are also indebted to Dr A. Pogany and Dr P. Paterson from the Royal Melbourne Institute of Technology for preparation of the silicon specimens for RHEED and to Dr Uchida for the TED Si specimen. One of us (GL) thanks Professor L. T. Chadderton for hospitality and CSIRO and the Max-Planck-Gesellschaft for financial support during the stay at the Division of Chemical Physics.

References

DOWELL, W. C. T. & WILLIAMS, D. (1980). *Micron*, **11** (Suppl. 1), 45.

GOODMAN, P. (1972). *Acta Cryst.* A**28**, 92-93.

HØJLUND-NIELSEN, P. E. & COWLEY, J. M. (1976). *Surf. Sci.* **54**, 340-354.

HSU, T. & COWLEY, J. M. (1983). *Ultramicroscopy*, **11**, 239-250.

ICHIMIYA, A., KAMBE, K. & LEHMPFUHL, G. (1980). *J. Phys. Soc. Jpn*, **49**, 684-688.

KOHRA, K., MOLIÈRE, K., NAKANO, S. & ARIYAMA, M. (1962). *J. Phys. Soc. Jpn*, **17**, (Suppl. B-II), 82–85.

LAUE, M. VON (1948). *Materiewellen und ihre Interferenzen*, 2nd ed., p. 357. Leipzig: Akademische Verlagsgesellschaft.

LEHMPFUHL, G. & REISSLAND, A. (1968). *Z. Naturforsch. Teil A*, **23**, 544–549.

LEHMPFUHL, G. & UCHIDA, Y. (1986). *Proc. Electron Microsc. Soc. Am.* pp. 376–379. San Francisco Press, Inc.

MARTEN, H. & MEYER-EHMSEN, G. (1985). *Surf. Sci.* **151**, 570–584.

OSAKABE, N., TANISHIRO, Y., YAGI, K. & HONJO, G. (1980). *Surf. Sci.* **97**, 393–408.

SHANNON, M. D., EADES, J. A., MEICHLE, M. E. & TURNER, P. S. (1985). *Ultramicroscopy*, **16**, 175–192.

TAFTØ, J. & LEHMPFUHL, G. (1982). *Ultramicroscopy*, **7**, 287–294.

UCHIDA, Y., JÄGER, J. & LEHMPFUHL, G. (1984). Proc. 8th Eur. Congr. Electron Microsc., pp. 567–568.

UCHIDA, Y., LEHMPFUHL, G. & JÄGER, J. (1984). *Ultramicroscopy*, **15**, 119–129.

VOSS, R., LEHMPFUHL, G. & SMITH, P. J. (1980). *Z. Naturforsch. Teil A*, **35**, 973–984.

Acta Cryst. (1986). A**42**, 577–585

Pendellösung Radiation and Coherent *Bremsstrahlung*

BY J. C. H. SPENCE AND G. REESE*

Department of Physics, Arizona State University, Tempe, AZ 85287, *USA*

(*Received* 14 *March* 1986; *accepted* 10 *July* 1986)

Abstract

The spontaneous emission process, which is kinematically forbidden in vacuum, may occur for kilovolt electrons traversing thin crystals as a direct result of the dynamical diffraction process which Paul Ewald was amongst the first to understand. The history of this effect is briefly reviewed. New experimental results, and the relevant theoretical background, are given for the resulting monochromatic X-ray emission lines known as coherent *Bremsstrahlung* and channelling radiation. The fine structure of these lines in particular is discussed, and their effects on electron energy-loss spectra described.

1. Introduction

'Having Ewald's theory as an example, it was easy to develop the theory of electron diffraction', wrote Hans Bethe in 1981. Guided by Ewald's ideas, Bethe thus developed the modern theory of dynamical electron diffraction, in which the absence of a vector field affords considerable simplification (Bethe, 1928). At a recent American Crystallographic Association meeting, Ewald reminisced on how he had developed his theory during off-duty hours in a horse-drawn ambulance during the First World War (Ewald, 1916). The discovery of electron diffraction from crystals in 1927 provided the incentive for the application of Ewald's work to charged particles. This paper outlines the way in which Bethe's theory of electron diffraction has become the basis of the modern theory of *Bremsstrahlung* from electrons traversing crystalline targets. Only comparatively recently has it been fully appreciated how profoundly the effects of dynamical diffraction influence the theory of *Bremsstrahlung* product in crystals, and how intimately the two effects are related. In brief, whereas the conventional theory of *Bremsstrahlung* for isolated atoms (due to Bethe and Heitler) predicts an emission spectrum which is continuous in energy up to a certain cutoff, the modern theory of *Bremsstrahlung* for 'low'-energy (<2 MeV) collimated electrons traversing a crystalline target predicts a series of monochromatic X-ray emission lines, one for each reciprocal-lattice vector and extinction distance. Since the energies and intensities of the lines are related to crystal structure factors, the resulting families of lines, known as coherent *Bremsstrahlung* (CB) and channelling radiation (CR), contain a great deal of crystal structure information. In the modern view, both CB and CR result from spontaneous emission between Bloch wave states of the incident beam. Only by taking these states to be solutions of the full three-dimensional dynamical diffraction problem, which Paul Ewald was amongst the first to understand, can the relationship between CB and CR be fully understood.

The purpose of this paper is to present experimental evidence for 'type B' coherent *Bremsstrahlung* lines from a new longitudinal mode in the zone axis (axial) orientation from diamond, and to provide the relevant theoretical background needed for its interpretation using the language of dynamical electron diffraction. Particular emphasis is placed on the crystal structure information in CB and CR. We also discuss the fine structure of these lines and the form of the electron energy-loss spectra to be expected from the CB and CR processes.

Channelling radiation was observed for the first time in 1975 (Vorobiev, Kaplin & Vorobiev, 1975),

* Motorola, Government Electronics Group, Scottsdale, AZ 85251, USA.

0108-7673/86/060577-09$01.50